Supplement of Atmos. Chem. Phys., 17, 3945–3961, 2017
http://www.atmos-chem-phys.net/17/3945/2017/
doi:10.5194/acp-17-3945-2017-supplement

Atmospheric Chemistry and Physics
Open Access

Supplement of

Biomass burning and biogenic aerosols in northern Australia during the SAFIRED campaign

Andelija Milic et al.

Correspondence to: Branka Miljevic (b.miljevic@qut.edu.au)

S1 Data analysis

High organic aerosol (OA) loadings during heavy biomass burning (BB) episodes interfered with sulfate detection by the AMS in unit mass resolution (UMR), resulting in negative sulfate readings and scattered data points (Fig. S1a). Adjustments in Squirrel to the fragmentation table addressed the negative data points (Fig. S1b), however significant data dispersion still remained. High resolution (HR) fitting using PIKA improved correlation among different sulfate fragments (Fig. S1c).

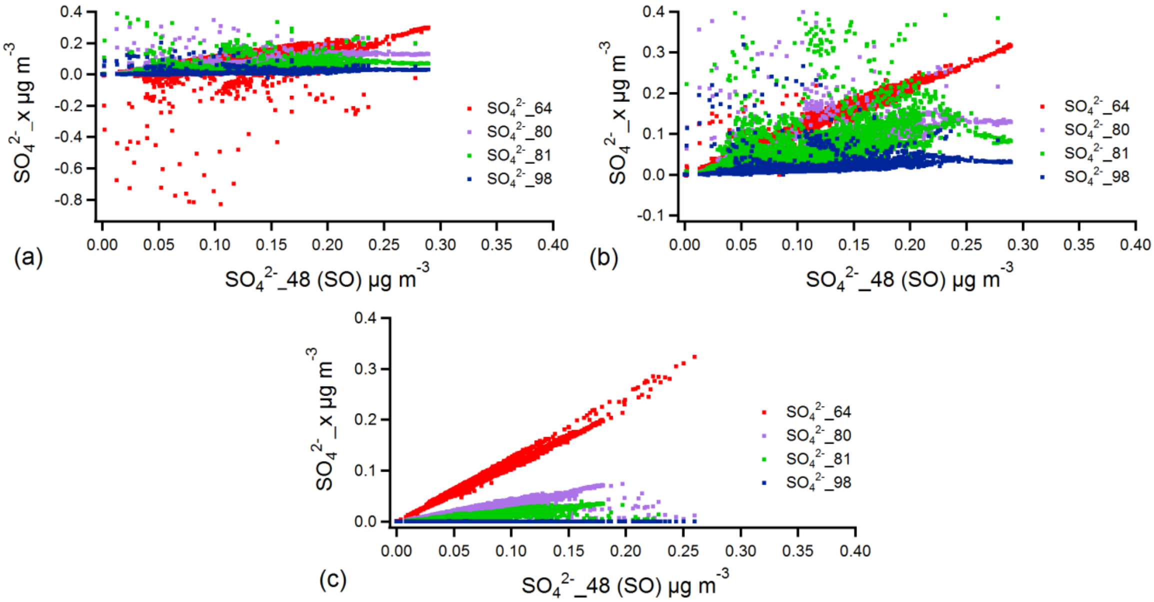

Figure S1: Sulfate fragments plots (a) before and (b) after Squirrel fragmentation table adjustments, and (c) after HR fitting in PIKA; SO_4^{2-}_x indicates sulfate fragments at m/z 64, 80, 81 and 96 plotted against the sulfate fragment at m/z 48.

PM1 soluble ions measured by ion suppressed chromatography and OM (converted from OC that was determined by the Thermal-Optical Carbon Analyser) were compared to the corresponding AMS UMR and HR data. A considerable improvement was observed in the HR analysis results for sulfate (Fig. S2b), with R changing from 0.4 to 0.8. HR fitting did not result in significant change for the other inorganic species or organics. However, improvement in the sulfate signals was significant and HR peak fitting data were used in further analysis.

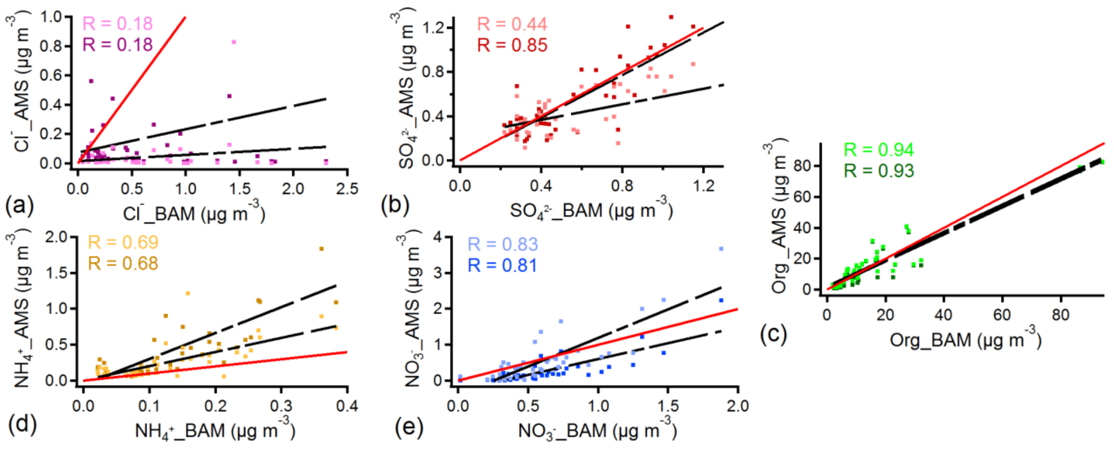

Figure S2: Correlation between BAM PM1 soluble ions and corresponding AMS species including (a) chloride, (b) sulfate, (c) OA, (d) ammonia and (e) nitrate; The lighter points and first number present correlation of BAM data with UMR AMS data, while the darker points and the second number illustrates the correlation for BAM and HR AMS data. Red line represents 1:1 line (absolute concentration between AMS and BAM). BAM organic mass (OM) was converted from OC mass using the conversion coefficient of 1.4. R refers to Pearson correlation coefficient. The AMS data were averaged to BAM 12h data.

Table S1: Correlation values between inorganic species and OA during the campaign, and close and distant periods separately. Inorganic species measured during the whole period (X), close BB periods (X(c)) and distant BB periods (X(d)) were compared to OA measured during the same time period (Org, Org(c), Org(d)).

	Cl^-	Cl^- (c)	Cl^- (d)	NH_4^+	NH_4^+ (c)	NH_4^+ (d)	NO_3^-	NO_3^- (c)	NO_3^- (d)	SO_4^{2-}	SO_4^{2-} (c)	SO_4^{2-} (d)
Org	0.65			0.92			0.75			0.55		
Org(c)		0.67			0.92			0.72			0.49	
Org(d)			0.47			0.73			0.77			0.48

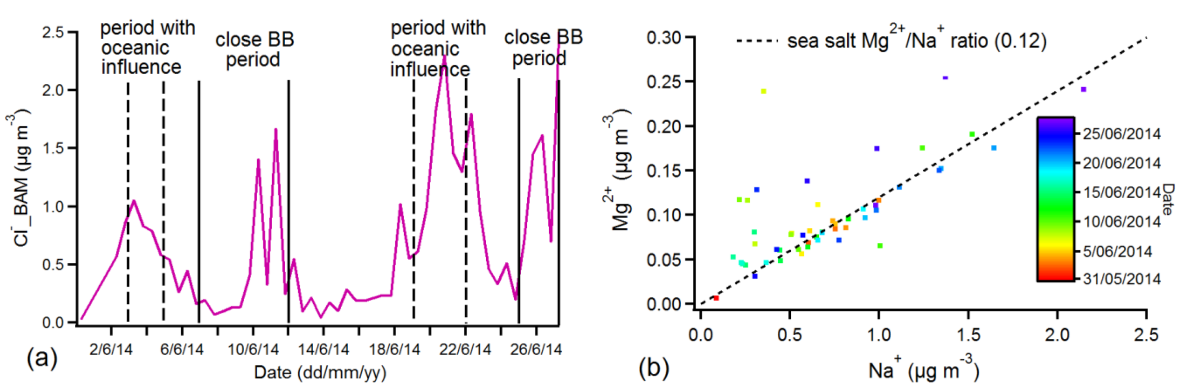

Figure S3: (a) Time series of chlorides collected on the filters (BAM). Dashed lines are defining the periods with oceanic influence, while solid lines illustrate close BB periods. (b) The filter (BAM) data for magnesium (Mg^{2+}) and sodium (Na^+). Black line illustrates Mg^{2+}/Na^+ ratio for the sea salt (0.12).

S2 Biomass burning aerosols and aging

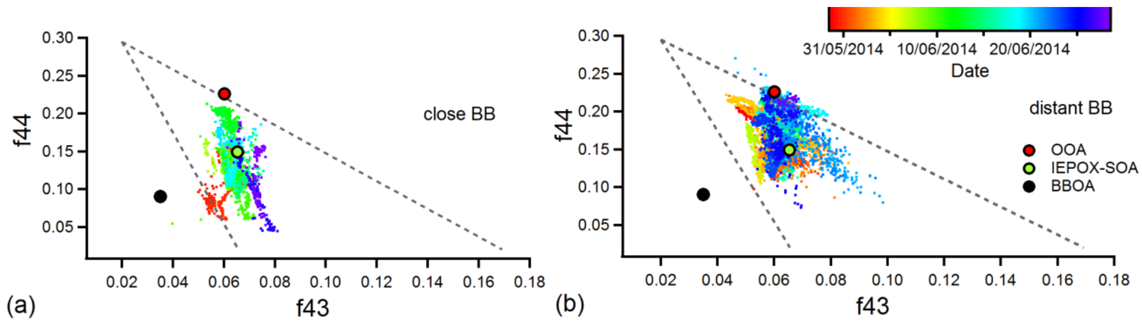

Figure S4: f44 vs. f43 coloured by date for (a) close and (b) distant BB periods. PMF-resolved factors are also indicated. The dashed lines represent boundaries for typical ambient aerosol as presented in Ng et al. (2010).

S2.1 Secondary organic aerosol (SOA) formation

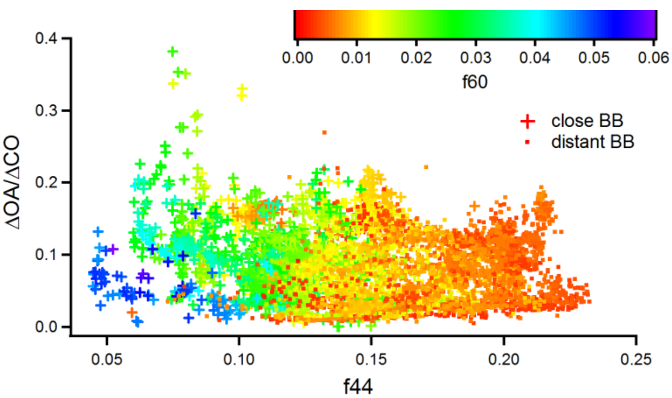

Figure S5: Change in ΔOA/ΔCO ratio with aging (represented by f44 values) for close (crosses) and distant (dots) fires coloured by f60.

S2.2 Biomass burning events

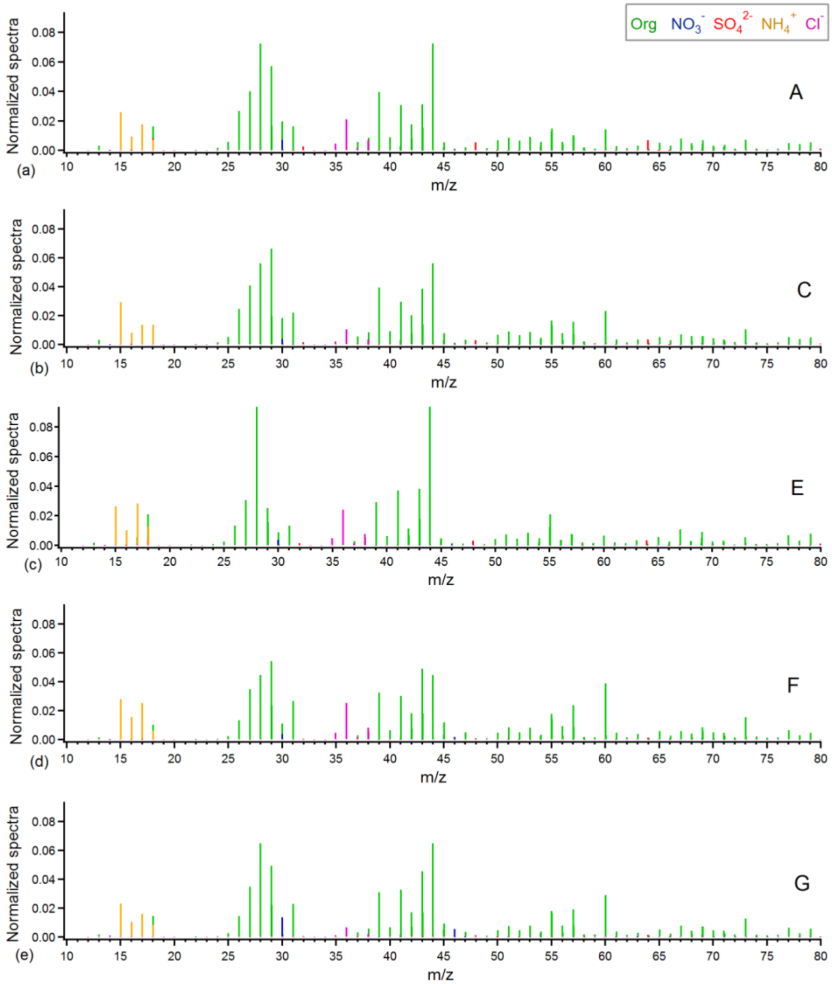

Figure S6: Normalised mass spectra (sum=1) for selected BB events (A (30/05/14, 18:34-19:25), C (30/05/14, 23:41-31/05/14 00:59), E (09/06/14, 19:45-10/06/14 00:32), F (25/06/14, 12:28-16:59) and G (25/06/14, 21:40-26/06/14 03:59) are shown respectively.

Sentinel hotspots and backtrajectories

On 30th of May at around 2pm three hot spots (two having confidence level of approximately 50% and one of 70%) were detected within 2km on the NE from the ATARS (Fig. S7a - Fig.S7d). These hot spots likely illustrated two fire events. On the same day and time, 11km on the SE from the sampling site, cluster of events was observed, including 4 hot spots with the confidence level between 94% and 100% and one of 78% confidence level. As all of them were spotted at the same time and within 1km distance, it is most likely that the one big fire has occurred. No other close events were observed over this time period. Cluster of hot spots was detected on the SE approximately 50km from the ATARS and big clusters at 100km and 150km, as well as on the SE. Moreover, 200km on E along the backtrajectories cluster of hot spots was observed.

On 25th of June three hotspot clusters were observed close to ATARS (2km on SE, 5km on NE and 10km on SE) (Fig. S7e-Fig. S7h). The cluster of hot spots observed 10 km from the sampling site had one of the highest hot spot's power (energy released by the fire) observed close to the ATARS (within 20 km) during the campaign (120 MW/km^2). Besides the close fires two big clusters around 60 km and 120 km on the SE from ATARS were detected on the same day.

On the 9th of June cluster of hot spots (all with the confidence level higher than 70%) was detected 5 km from ATARS. Number of distant hot spots was detected between 100 km and 200 km, on the SE from the ATARS.

Backtrajectories for all BB Events are given at Fig. S7.

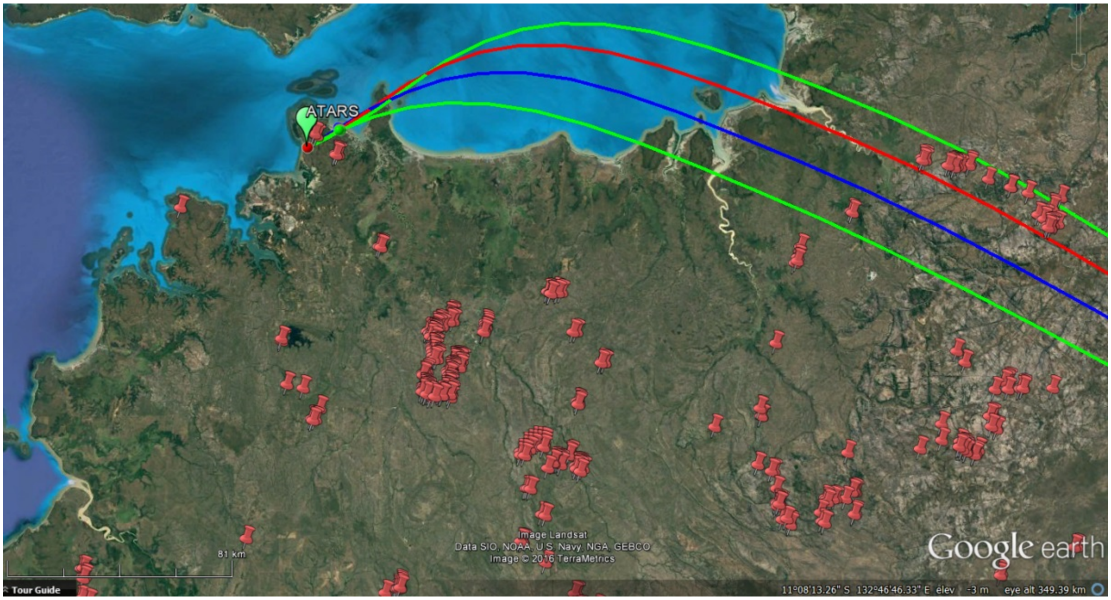

(a)


ATARS

(b)

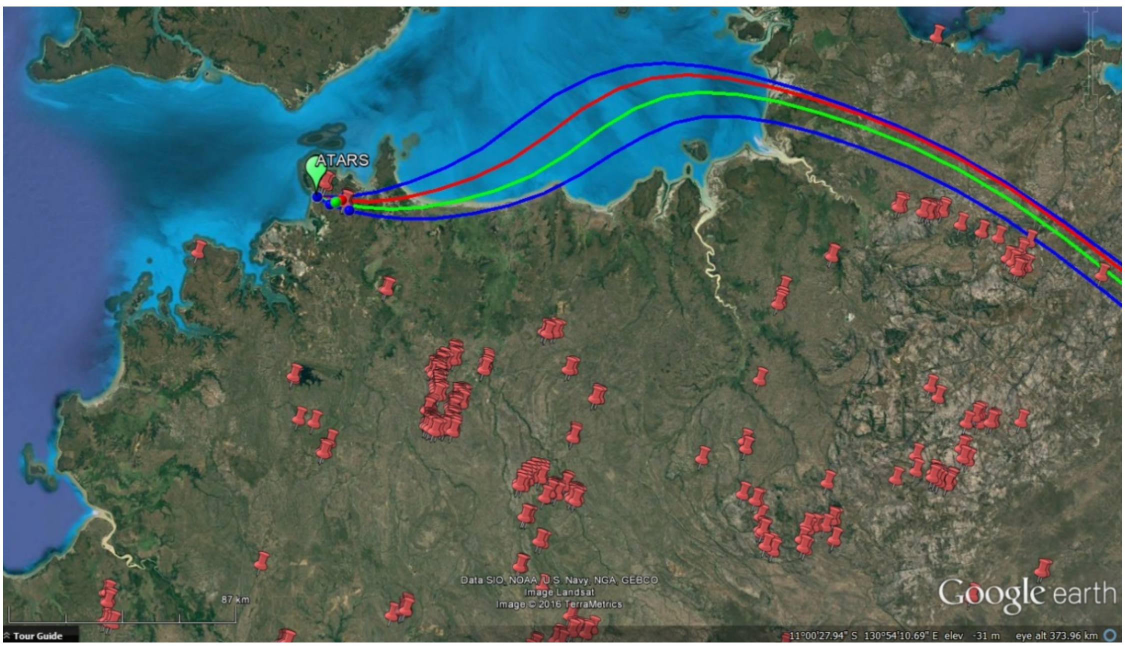
ATARS
Data SIO, NOAA, U.S. Navy, NGA, GEBCO
Image Landsat
Image © 2016 TerraMetrics
Google earth
87 km
Tour Guide

(c)

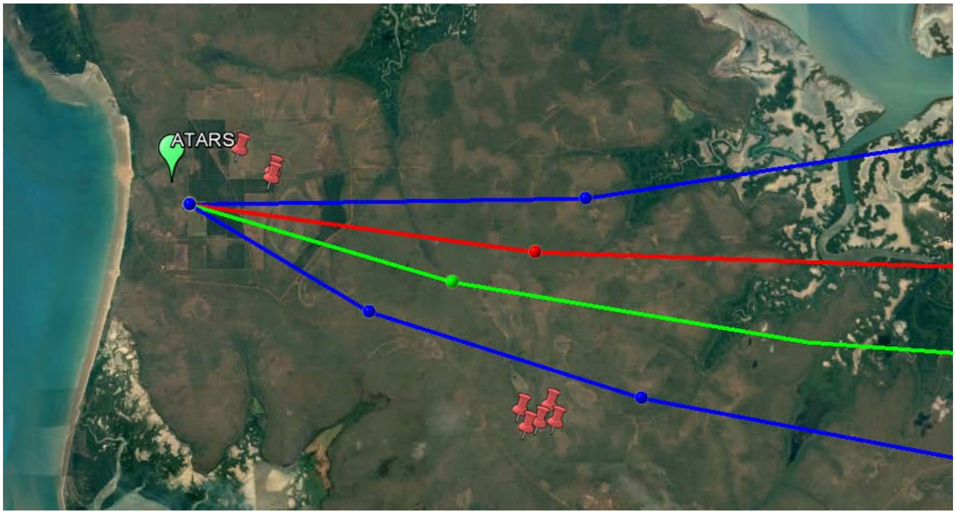
ATARS

(d)

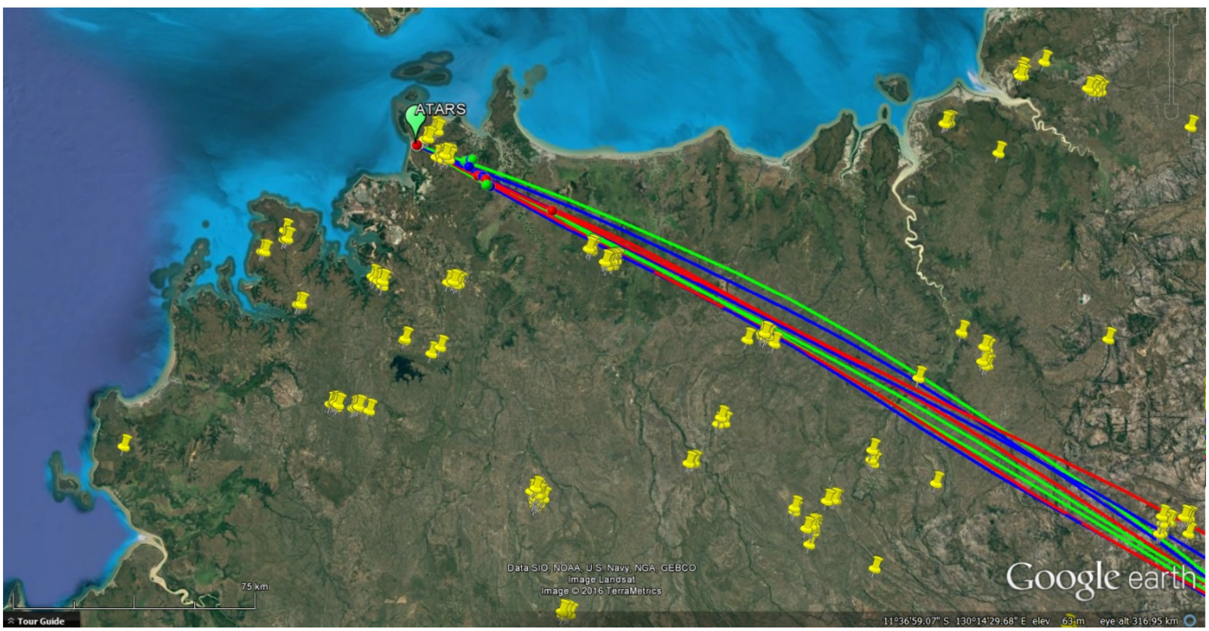
ATARS
75 km
Tour Guide
Data SIO, NOAA, U.S. Navy, NGA, GEBCO
Image Landsat
Image © 2016 TerraMetrics
Google earth
11°36'59.07" S 130°14'29.68" E elev 63 m eye alt 316.95 km

(e)

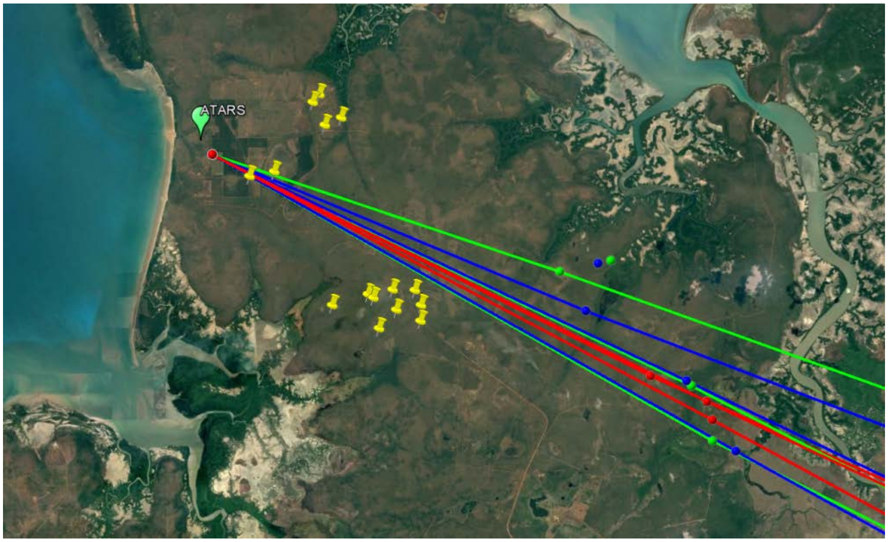
ATARS

(f)

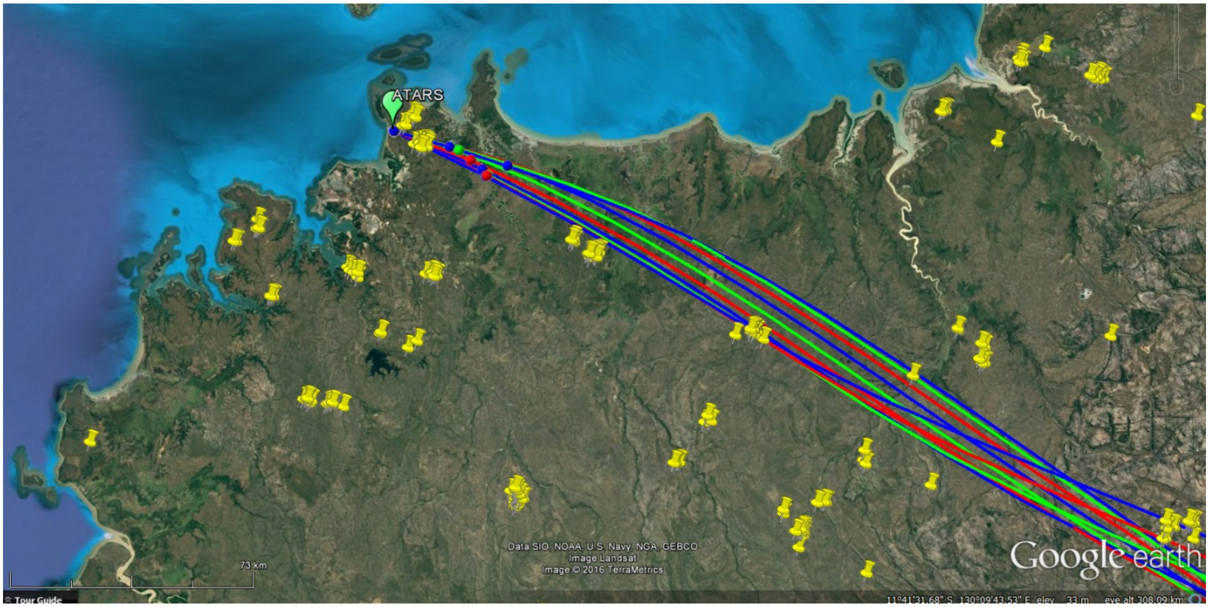
ATARS
Data SIO, NOAA, U.S. Navy, NGA, GEBCO
Image Landsat
Image © 2016 TerraMetrics
73 km
Google earth

(g)

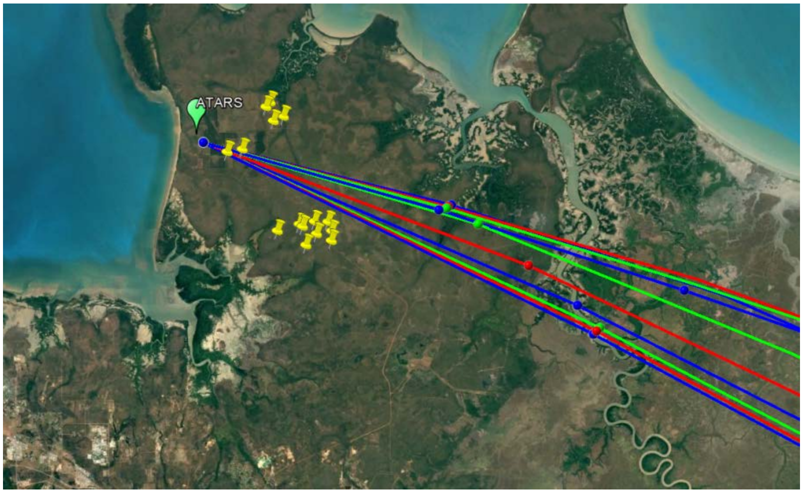
ATARS

(h)

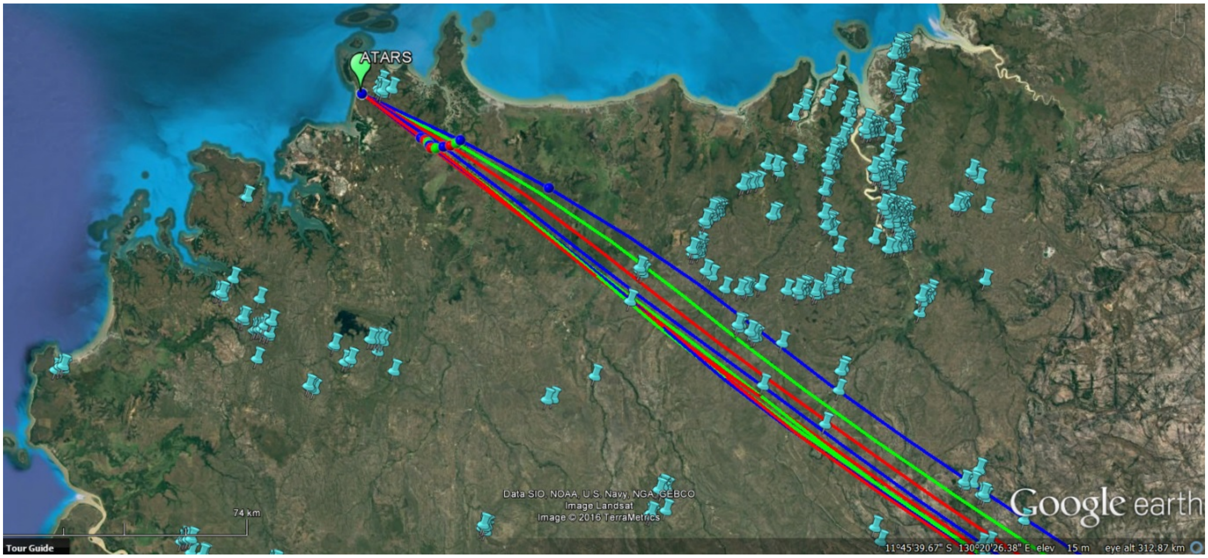
ATARS
Data SIO, NOAA, U.S. Navy, NGA, GEBCO
Image Landsat
Image © 2016 TerraMetrics
74 km
Google earth
Tour Guide

(i)

(j)

Figure S 7: Backtrajectories for Event A, with close hot spots (a) and close and distant hot spots (b), for Event C, with close hot spots (c) and close and distant hot spots (d), for Event F, with close hot spots (e) and close and distant hot spots (f), for Event G, with close hot spots (g) and close and distant hot spots (h) and for Event E, with close hot spots (i) and close and distant hot spots (j). The backtrajectories were computed using the HYSPLIT (Hybrid Single-Particle Lagrangian Integrated Trajectory) model. All backtrajectories were run for 24h back in time. Different colours illustrate different starting time. (Google Earth V 7.1.2.2041; December 5, 2016; Northern Territory, Australia).

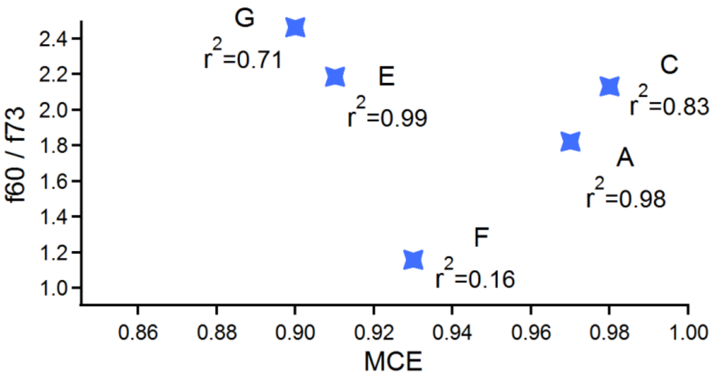

Figure S 8: f60/f73 ratio vs. modified combustion efficiency (MCE) for different events. Each point label indicates name of event and correlation value between f60 and f73.

S3 PMF performed on the whole dataset

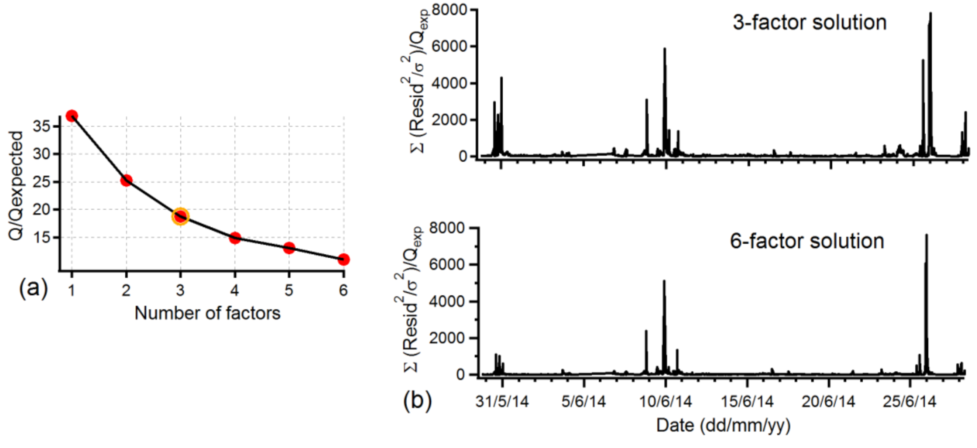

Figure S9: (a) Q/Qexpected (Q refers to the sum of squared scaled residuals over the whole dataset) vs. number of factors, illustrating high error and residual values. (b) Time series of Q/Q expected contribution for 3 and 6-factor solutions where it is clear that higher number of factors does not make the residual structure during BB events significantly lower.

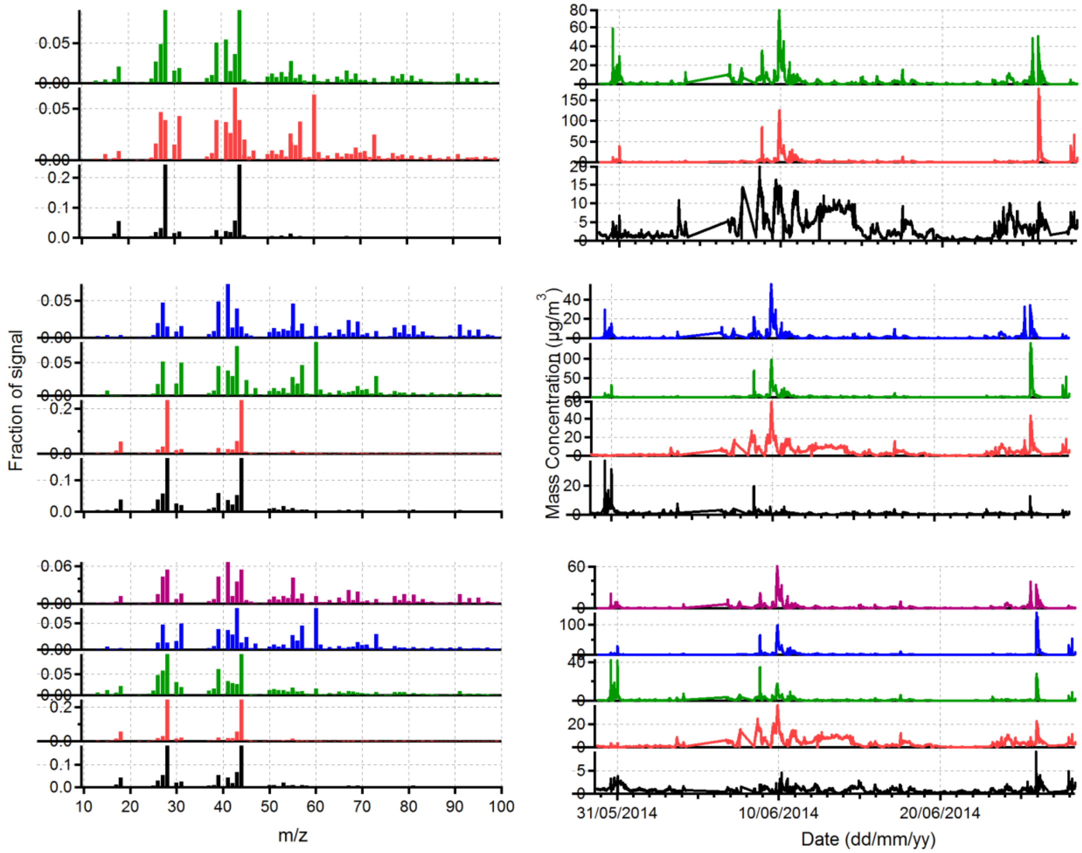

Figure S10: Factor profiles and time series for 3, 4 and 5-factor solutions showing BBOA factor splitting, suggesting that plumes are apportioned to different PMF factors.

S4 PMF performed on the background dataset

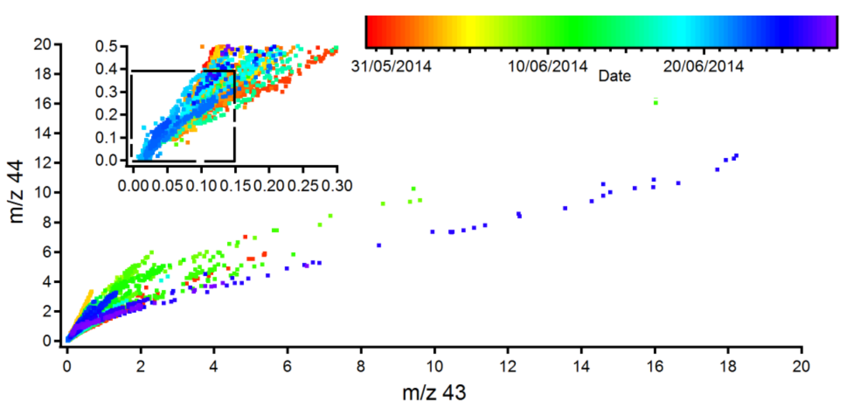

Figure S11: m/z 44 vs. m/z 43 coloured by date for the whole dataset and for background periods (inset). Black dashed box in inset graph illustrates cut-offs of 0.15 for m/z 43 and 0.4 for m/z 44 chosen for background data.

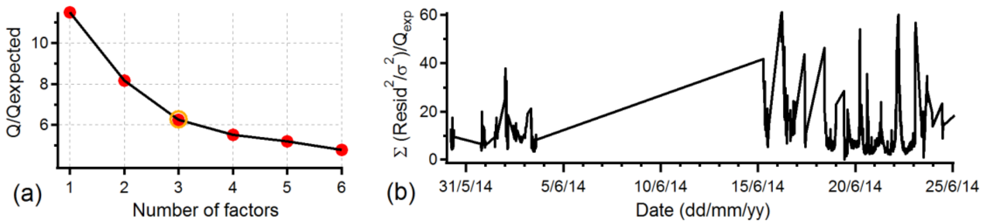

Figure S12: (a) Q/Qexpected vs. number of factors and (b) time series of Q/Q expected contribution for the 3-factor solution illustrating significantly smaller residuals in the case of the background dataset, compared to the whole dataset.

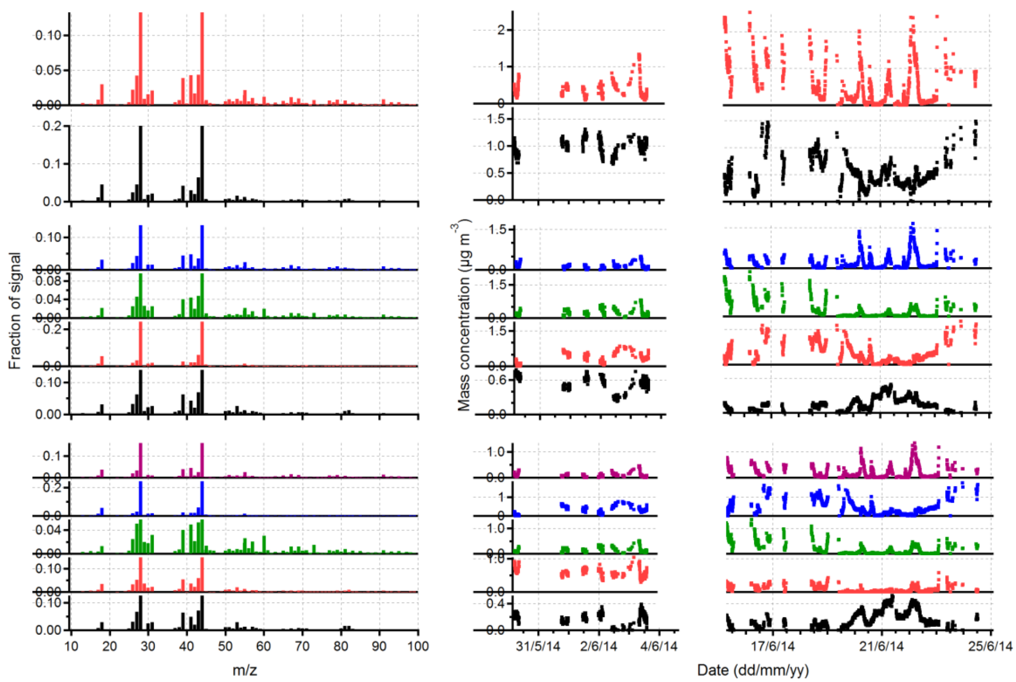

Figure S13: Factor profiles and time series for 2, 4 and 5-factor solutions for the background dataset.

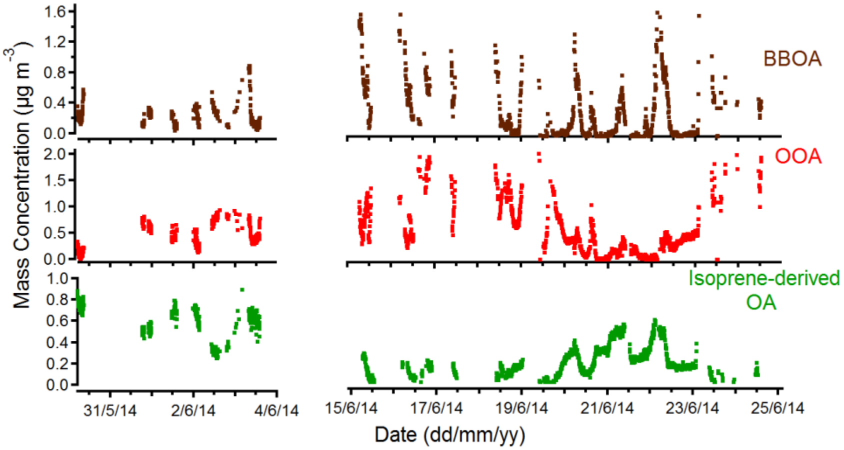

Figure S14: Time series for 3-factor solution for the background dataset.

S4.1 Isoprene-derived- organic aerosol

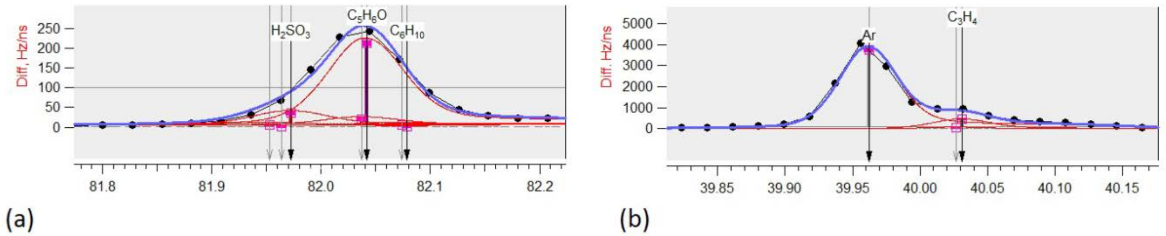

Figure S15: HR peak fitting at (a) m/z 82 showing the dominance of the $C_5H_6O^+$ fragment and (b) m/z 40 demonstrating good m/z calibration.

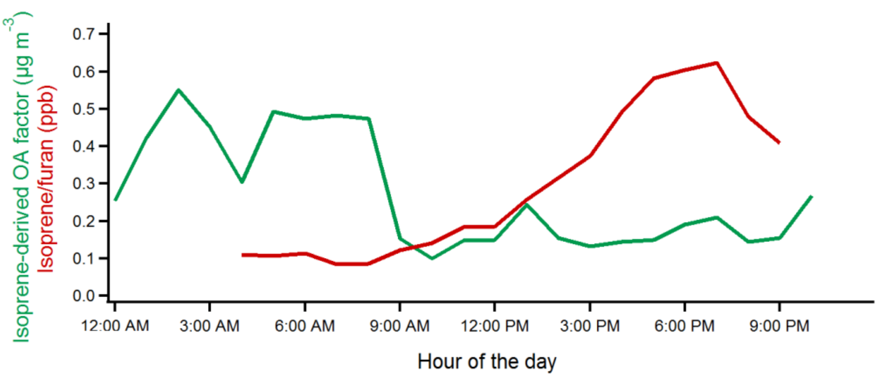

Figure S16: Diurnal trend of PMF IEPOX-SOA factor and isoprene/furan concentration measured by PTR-MS.

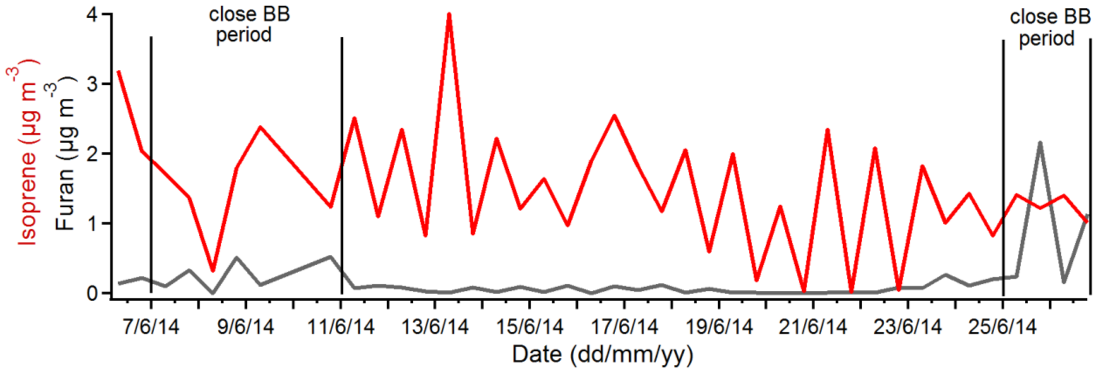

Figure S 17: Time series of isoprene and furan concentrations analysed by the gas chromatography-mass spectrometry. Black lines illustrate close BB periods.